Version of Record: https://www.sciencedirect.com/science/article/pii/S0022309322000011
Manuscript_1aef944cb9a223101902016e0d73f6a2

Structure and Fragility of Zn-phosphate glasses: Results from multinuclear NMR spectroscopy and calorimetry

[1]Yiqing Xia, [1]Hao Chen, [2]Ivan Hung, [2]Zhehong Gan, [1]Sabyasachi Sen*

[1]Department of Materials Science & Engineering, University of California at Davis, Davis, CA 95616, USA

[2]National High Magnetic Field Laboratory, 1800 East Paul Dirac Drive, Tallahassee, Florida 32310, USA

*Corresponding Author: Sabyasachi Sen (email: sbsen@ucdavis.edu)

Abstract

The structure of $(ZnO)_x(P_2O_5)_{100-x}$ glasses with $35 \leqslant x \leqslant 67$ is investigated using ^{31}P and ultra-high field ^{67}Zn NMR spectroscopy. The ^{31}P NMR results confirm a nearly binary Q-species distribution. The progressive decrease in the connectivity of the phosphate network upon addition of ZnO is manifested in a monotonic drop in T_g in the composition range $35 \leqslant x \leqslant 55$. The ^{67}Zn NMR spectra indicate that the average Zn-O coordination number varies between 4 and 6 and increases progressively with increasing Zn content. The resulting increase in the connectivity of the Zn-O-P network compensates for the depolymerization of the P-O-P network, which is reflected in a reversal in the compositional trend in T_g for $x>55$. In contrast to T_g, the fragility index m shows negligible composition dependence until x~50, beyond which it increases rapidly with increasing Zn content in response to the progressive shortening of the Q^2 chains.

1. Introduction

Zinc phosphate glasses are characterized by a large composition range for glass formation, high solubility of rare earth ions, relatively high thermal expansion coefficient and good durability, which make them viable candidates for a wide range of applications in the areas of composites, optical waveguides, lasers and amplifiers and hermetic glass-to-metal seals [1–6]. Consequently, the atomic structure-property relationships in these glasses have been investigated in detail over the last decades [7–14]. These studies have shown that progressive addition of ZnO to P_2O_5 leads to a monotonically depolymerizing phosphate network where the PO_4 groups closely follow van Wazer's reorganization model of binary speciation. However, such a monotonic evolution of the phosphate network as such cannot explain the strongly non-monotonic compositional variation in properties such as the glass transition temperature T_g and density ρ of Zn-phosphate glasses, both of which display a minimum near the metaphosphate composition with 50 mol% ZnO. This behavior led Kordes et al. to classify Zn-phosphates as "anomalous" glasses [15]. These authors hypothesized that such a non-monotonic behavior of T_g and ρ may be related to a change in the Zn coordination environment, where the Zn-O coordination number (CN) increases from 4 to 6 with increasing Zn content across the metaphosphate composition. More recently, Tischendorf et al. [12] have also argued that this increase in Zn CN increases the connectivity of the structural network in Zn-phosphate glasses with >50 mol% ZnO, which more than compensates for the depolymerization of the phosphate network and thus, can lead to an increase in T_g with increasing ZnO content.

Previous X-ray and neutron diffraction studies, on the other hand, have shown that the Zn atoms are tetrahedrally coordinated in Zn-phosphate glasses with ≥40 mol% ZnO, irrespective of the ZnO content [7]. In contrast, in ultraphosphate glasses progressive lowering of the ZnO

content was reported to lead to a slow increase of the Zn CN to ~6 [16]. A careful analysis of the Zn-O peak in the X-ray and neutron real-space correlation function by Walter et al. [7] has shown that the Zn CN increases only slightly, from ~ 4.0 to ~ 4.2 with increasing Zn content beyond 60 mol%. Previous molecular dynamics simulation studies [11] have also indicated a compositionally invariant Zn CN of ~ 4 in Zn-phosphate glasses with 70 mol% ≥ ZnO ≥ 40 mol%. Therefore, the aforementioned non-monotonic compositional variation of T_g and ρ was argued to be unrelated to a concomitant change in the Zn CN. Hoppe and coworkers [7,16], have proposed an alternate model on the basis of diffraction studies where the Zn CN remains unchanged, however, the connectivity of the ZnO_4 coordination polyhedra changes from isolated tetrahedra in the metaphosphates to corner- and edge- shared tetrahedra in glasses with >50 mol% ZnO. This increase in the connectivity between the ZnO_4 tetrahedra results in an increase in the packing density of the structural network as well as compensates for the depolymerization of the phosphate network, giving rise to a concomitant increase in T_g. However, an unequivocal structural origin of this intriguing non-monotonic behavior of physical properties in Zn-phosphate glasses remains missing to date, which warrants direct high-resolution probing of the composition dependence of Zn coordination environment in these glasses.

Recently, high-field ^{67}Zn nuclear magnetic resonance (NMR) spectroscopy has been shown to be a powerful technique in studying Zn coordination environments in metal-organic-framework glasses [17]. Moreover, the ^{67}Zn NMR isotropic chemical shift δ_{iso} has been shown to be sensitive to the coordination environment of Zn atoms in various crystalline oxides [18,19]. In spite of such promise, high-resolution NMR spectroscopy of the ^{67}Zn nuclide remains rather challenging, owing to its low gyromagnetic ratio and low natural abundance in combination with its large quadrupole moment [17]. These issues necessitate the use of ultra-high magnetic fields

(≥20 T) and the application of experiments such as two-dimensional (2D) quadrupolar magic-angle-turning (QMAT) NMR [20] to avoid the interference from spinning sidebands in the acquisition of high-resolution ^{67}Zn central-transition magic-angle-spinning (MAS) NMR spectra. Here we present the results of a ^{31}P MAS and ultra-high magnetic field (up to 35.2 T) ^{67}Zn QMAT NMR spectroscopic study of the structure of Zn-phosphate glasses with 35 mol% ≤ ZnO ≤ 67 mol%. The structural evolution is shown to be consistent with the compositional variation of molar volume, T_g and activation energy of viscous flow at T ~ T_g, i.e., the fragility index of these glasses.

2. Experimental methods

2.1. Sample preparation and physical characterization

The $(ZnO)_x(P_2O_5)_{100-x}$ glasses with 35≤ x ≤67 were prepared by conventional melt-quenching method. Appropriate amounts of $NH_4H_2PO_4$ (99.9%, Acros Organics) and ZnO (99.99%, Alfa Aesar) were mixed and loaded in alumina crucibles. The mixtures were first calcined at 450°C overnight to remove any water and ammonia. The calcined batches were subsequently melted at 1200°C for 1.5h and then quenched by flowing nitrogen gas. The as-made glass samples were stored in a desiccator to avoid exposure to atmospheric moisture.

The T_g of these $(ZnO)_x(P_2O_5)_{100-x}$ glasses was determined using differential scanning calorimetry (Mettler Toledo DSC1). Samples of mass ~15-20 mg were taken in hermetically sealed Al pans and were heated to 50 °C above T_g to erase any thermal history. The samples were then cooled in the calorimeter at a rate of 10K/min and subsequently reheated at the same rate. The fictive temperature T_f was taken as the peak of the endothermic glass transition signal while heating the

sample at a specific rate q K/min ranging from 0.5 to 30 K/min, subsequent to cooling at the same rate from T_g+30K to T_g−50K. The T_g was determined to within ± 2 °C as the onset of the glass transition endotherm at a heating rate of 10 K/min. On the other hand, the dependence of T_f on q yields the activation energy E for enthalpy relaxation according to the relation: $\frac{d \ln q}{d(\frac{1}{T_g})} = -\frac{E}{R}$. The fragility index m was determined from E using the relation $m = \frac{E}{RT_g \ln 10}$ [21].

Density of these glasses was measured using a gas expansion pycnometer (Micromeritics AccuPyc II 1340) at 20°C using helium (6N purity) as the displacement gas. For each measurement, approximately 0.5 g of glass sample was loaded into a 1 cm^3 cup. All reported density values are averages of 10 consecutive measurements of each sample.

2.2. ^{31}P NMR measurements

The ^{31}P MAS NMR spectra of all glasses were collected using a Bruker Avance-500 spectrometer equipped with a 11.7 T magnet (^{31}P Larmor frequency of 202.4 MHz). Crushed glass samples were taken in 4 mm ZrO_2 rotors and were spun at 15 kHz using a Bruker triple-resonance MAS probe. Each ^{31}P MAS spectrum is the Fourier transform of 64 free induction decays acquired with using a single pulse with a pulse length of 0.85 μs (tip angle = 45°) and a recycle delay of 60 s. All ^{31}P spectra were externally referenced to Na_2HPO_4 with δ_{iso} at 4.6 ppm. The spectral line shapes of ^{31}P MAS NMR experiments were analyzed using the software DMFit [22]. The three principal components of the second-rank NMR chemical shift tensor δ_{xx}, δ_{yy} and δ_{zz}, can be recast into the isotropic shift δ_{iso}, and the magnitude Δ and asymmetry η of the chemical shift anisotropy (CSA). Following the Haeberlen convention $|\delta_{zz} - \delta_{\mathrm{iso}}| \geq |\delta_{xx} - \delta_{\mathrm{iso}}| \geq |\delta_{yy} - \delta_{\mathrm{iso}}|$, these quantities are defined as:

$\delta_{\text{iso}} = \frac{1}{3}(\delta_{zz} + \delta_{xx} + \delta_{yy})$,

$\Delta = \delta_{zz} - \delta_{\text{iso}}$,

$\eta = \frac{\delta_{yy} - \delta_{xx}}{\Delta}$,

It may be noted that Δ and η represent the deviation of the tensor from spherical and uniaxial symmetry, respectively.

2.3. ^{67}Zn QMATPASS/QCPMG NMR spectroscopy

The ^{67}Zn QMATPASS/QCPMG NMR spectra of the Zn-phosphate glasses were acquired at the National High Magnetic Field Laboratory (NHMFL, Tallahassee, Florida, USA), using Bruker Avance NEO consoles and 3.2 mm probes designed and constructed at the NHMFL. Only select glass compositions were measured due to long acquisition time needed and the limited availability of the ultra-high field (35.2 T) series-connected hybrid (SCH) magnet [23]. Two-dimensional ^{67}Zn spectra were obtained using the QMAT pulse sequence [20], and signal enhancement via the multiple-echo QCPMG acquisition scheme [24]. For spectra acquired at 35.2 T corresponding to a ^{67}Zn Larmor frequency of $\nu_0(^{67}\text{Zn})$ = 93.9 MHz, central-transition selective π/2- and π-pulses of 2.5 and 5.0 μs were used with an *rf* field of 33.3 kHz, MAS sample spinning frequency of 16 kHz, 8 hypercomplex t_1 increments with 49200 transients per increment, 14 CPMG echoes per transient, and a 20 ms recycle delay for a total experimental duration of 6.6 hours per spectrum. For spectra acquired at 19.6 T ($\nu_0(^{67}\text{Zn})$ = 52.0 MHz), central-transition selective π/2- and π-pulses of 5.0 and 10.0 μs were used with an *rf* field of 16.7 kHz, 16 kHz MAS, 8 hypercomplex t_1 increments with 490000 transients per increment, 14 CPMG echoes per transient, and a 30 ms recycle delay for a total experimental duration of 119.4 hours per spectrum. Hypercomplex data acquisition was performed by applying the method of

States et al. [25] to the QCPMG pulse phase and the receiver phase simultaneously. The QCPMG echoes were summed before 2D Fourier transformation. 'Center-band only' spectra were obtained by a shear transformation as for MAT/CPMG spectra [26], to align the spinning sidebands separated along the indirect dimension, followed by summation of all the sidebands. ^{67}Zn spectra were externally referenced by recording the ^{17}O signal of D_2O and using the ^{17}O and ^{67}Zn frequency ratios reported in the IUPAC recommendations [27].

3. Results and Discussion

The ^{31}P MAS NMR spectra of the $(ZnO)_x(P_2O_5)_{100-x}$ glasses with $35 \leqslant x \leqslant 67$ are shown in Fig. 1. While the center bands of the ^{31}P MAS NMR spectra in Fig. 1 correspond to the isotropic shifts of the various PO_4 tetrahedral species in the glass structure, denoted as Q^n with n being the number of bridging oxygen atoms, the spinning sidebands originate from the CSA of these species and thus contain information on the anisotropic parameters Δ and η. The center-band and sidebands of these spectra were simulated using Gaussian peaks with δ_{iso} = 4±1, −13±2, −30±3, and −41±4 ppm corresponding, respectively, to the Q^0, Q^1, Q^2 and Q^3 species, and with full-width-at-half-maximum of 12±3 ppm (Fig. 2). These simulations yield the relative abundance of the constituent Q^n species from their respective peak areas including the sidebands, and their characteristic chemical shift tensor parameters Δ and η. It is clear from Fig. 1 that both the isotropic (center-band) signal as well as the sideband pattern and intensity distribution change progressively with composition, indicating a corresponding evolution of the Q^n speciation. The center-band displays an increase in relative intensity on the high ppm side with increasing ZnO content, corresponding to a progressive replacement of the Q^3 species with Q^2 and subsequently with Q^1 species (see below). The experimentally determined relative fractions of the Q^n species are generally in good agreement with those predicted by van Wazer's binary Q-

speciation model (Fig. 3), with small deviations at the highest ZnO contents that can be attributed to the speciation reaction: $2\ Q^1 \rightarrow Q^2 + Q^0$. The resulting ratio of bridging:non-bridging oxygen (BO:NBO) atoms in the structure of these glasses agrees well with that expected from the nominal chemical composition of this glass over most of the composition range though the experimental values fall slightly below the expected trend for ultraphosphates with ≤ 45 mol% ZnO (Fig. 4). Such a deviation could result from the presence of some residual water in these glasses.

The compositional variation of the Δ and η parameters for the Q^1, Q^2 and Q^3 species obtained from simulation of the ^{31}P MAS NMR spectra are shown in Figs. 5 and 6. It is noteworthy that while Δ is relatively small and positive for the Q^1 species, it is large and negative for the Q^2 and Q^3 species. A similar variation in the sign of Δ is also well known for ^{29}Si in corresponding silicate Q species [28]. More interestingly, however, the Δ and η of Q^1 and Q^3 species appear to be nearly independent of composition within experimental error, while for the Q^2 species Δ shows a relatively rapid and monotonic decrease in magnitude with Zn content in glasses with >50 mol% ZnO (Figs. 5 and 6). We argue that this observation is indicative of a conformational change of the Q^2 chains as they progressively shorten with increasing Zn content in polyphosphate glasses. Such conformational changes may result in a more efficient packing for shorter chains due to a lowering of steric hindrance towards folding. Indeed, in previous studies Hoppe and coworkers [7,16] hypothesized that the "anomalous" increase in density with increasing Zn content in this compositional regime is likely a result of tighter packing of the constituent Q^2 chains.

The 1D ^{67}Zn 'center-band only' central-transition NMR spectra obtained from 2D QMATPASS/QCPMG at 35.2 and 19.6 T for the $(ZnO)_{40}(P_2O_5)_{60}$ glass sample are shown in Fig.

7. These spectra are characterized by asymmetric central-transition line shapes with low-frequency tails that are typical of quadrupolar nuclides in structurally disordered solids such as glasses with a continuous distribution of quadrupolar coupling constants C_Q. Such central-transition NMR line shapes are typically simulated with a Czjzek distribution of the quadrupolar tensor parameters along with a Gaussian distribution of δ_{iso} [22]. It may be noted that such a simulation procedure for the central-transition NMR spectra of quadrupolar nuclides in glasses collected at a single magnetic field may not yield a unique solution for the average C_Q and δ_{iso}, if the broadening due to the quadrupolar interaction and the chemical shift distribution are comparable. Instead, simultaneous simulation of NMR spectra acquired at significantly different magnetic fields helps constrain the relative magnitudes of these interactions. This is because in units of frequency the chemical shift broadening is proportional to the magnetic field, while the quadrupolar broadening is inversely proportional to the field. The ^{67}Zn NMR spectra at the two different fields in Fig. 7 have similar line widths when compared in units of ppm, which is highly unusual since spectra that are predominantly broadened by the quadrupolar interaction should have line widths in Hertz that are inversely proportional to the external magnetic field. At the magnetic fields of 35.2 and 19.6 T, this should translate into a reduction in line width at the higher field by a factor of $(35.2/19.6)^2 = 3.2$ in units of ppm. Therefore, the similar line widths in ppm indicate that a distribution of ^{67}Zn isotropic chemical shift or the presence of more than one distinct type of Zn site must be a major contributor to the appearance of the spectra in addition to the typical quadrupolar broadening. However, it may be noted that compared to the spectrum collected at 35.2 T, the 19.6 T ^{67}Zn NMR spectrum is broader near the low-frequency tail region, which suggests that a satisfactory simulation of the ^{67}Zn NMR line shapes would require the consideration of two overlapping signals, with the component at lower frequency being

characterized by a larger C_Q. The NMR program ssNake [29] was used to simultaneously fit the two ^{67}Zn NMR spectra in Fig. 7 employing the Czjzek model. The fit, though possibly non-unique, reproduces the experimental line shapes well, where one of the two Zn sites is characterized by δ_{iso} ~ 66 ppm and an average C_Q ~ 3.0 MHz and the other by δ_{iso} ~ 0 ppm with average C_Q ~ 4.0 MHz. Moreover, the average ^{67}Zn δ_{iso} obtained from these simulations are rather consistent with those reported for Zn in tetrahedral and octahedral coordination environment with oxygen in various compounds [18]. For example, the ZnO_4 tetrahedral environment in the compound $Zn(OAc)_2$ with Zn-O distances ranging between 1.95 and 1.97 Å is characterized by a ^{67}Zn δ_{iso} of 67 ppm [18]. A Zn-O distance of ~1.95 Å was indeed reported for Zn-metaphosphate glass and crystal in previous X-ray and neutron diffraction, Zn K-edge extended X-ray absorption fine structure spectroscopy and X-ray anomalous scattering studies [7,30]. It is important to contrast this result with the ZnO_4 tetrahedral environment in hexagonal ZnO with significantly longer Zn-O distances (2.33-2.39 Å), which is characterized by a ^{67}Zn δ_{iso} of 240 ppm [18,19]. On the other hand, the ZnO_6 octahedral environment in the compound $Zn(OAc)_2.2H_2O$ is characterized by a ^{67}Zn δ_{iso} of 0 ppm [18]. This two-site simulation is also found to be adequate to consistently model the ^{67}Zn QMAT central-transition NMR spectra of Zn-phosphate glasses with 60 and 67% ZnO (Fig. 8). The corresponding simulation parameters are listed in Table 1, which indicate that while the δ_{iso} and the average C_Q for these two sites do not change significantly with glass composition, the relative fraction of the high-frequency component corresponding to the ZnO_6 environment systematically increases from ~50% to ~ 70% as the ZnO content increases from 40 to 67 mol% (see Table 1). This trend is consistent with the shift of the center of gravity for the overall ^{67}Zn NMR line shapes towards higher frequencies with increasing Zn content (Fig. 8). When taken together, these results suggest a continuous

increase in the average Zn CN in these Zn-phosphate glasses with increasing Zn content. As has been noted above, this increase in the Zn CN with increasing Zn content in polyphosphates can compensate for the depolymerization of the phosphate network and increase its net connectivity. It should be emphasized that extraction of NMR parameters for two distinct Zn sites in these glasses would be considerably more ambiguous (maybe even impossible) without the large difference in magnetic field afforded by the 36 T SCH magnet compared to typically accessible NMR systems.

The compositional variation of T_g and of molar volume for these glasses as determined in the present study and in a number of previous studies are shown in Figs. 9 and 10, which are indeed consistent with the structural evolution observed in this study. In general, the T_g of a glassy network depends on the degree of connectivity of the network and the strength of the bonds that constitute the network. The decrease in T_g with increasing Zn in the composition region 35 mol% $\leq$ ZnO $\leq$ 55 mol% can thus be ascribed to the loss of connectivity from progressive depolymerization of the phosphate network. The depolymerization of the phosphate network results in a collapse of the network and a concomitant increase (decrease) in the atomic packing (molar volume). Further increase in ZnO content beyond 55% results in an increase in T_g, which can be attributed to a net increase in the network connectivity due to an increase in the Zn CN, despite the continuing depolymerization of the phosphate network and shortening of Q^2 chains. As hypothesized originally by Hoppe and coworkers [7,16] and evidenced in the variation of Δ and η of the Q^2 species in this composition regime (Figs. 5 and 6), the Q^2 chain shortening results in a lowering of steric hindrance to packing, which in combination with the increase in Zn CN gives rise to a marked increase in the rate of molar volume decrease in glasses with > 55 mol% ZnO (Fig. 10).

The compositional variation of the fragility index m of these Zn-phosphate glasses is shown in Fig. 11 and is compared with that for the Na-phosphate glasses, as reported in the literature [31]. It is interesting to note that while m for the Na-phosphate glasses starts to rise rapidly upon increasing the Na_2O content beyond 35 mol% (Fig. 11), for Zn-phosphates the onset of the rising trend is located at the metaphosphate composition (>50 mol% ZnO). The fragility trend displayed by the Na-phosphates has recently been explained by Sidebottom and coworkers using the coarse-graining model (CGM) [32–36]. This model attempts to establish a universal relationship between m and the network connectivity $<n>$ in glass-forming liquids on the basis of the relationship $\propto \left(\frac{dS_{conf}}{d<r>}\right)^2$. The term $\left(\frac{dS_{conf}}{d<n>}\right)$ represents the dependence of configurational entropy S_{conf} of a network on its connectivity, which, for chains with various degrees of cross-linking has been investigated in detail in the polymer literature using the self-avoiding walk model. Sidebottom [32] used this model to estimate the change in the conformational entropy of a disjointed chain of monomers, upon progressive addition of cross-links, as a function of the length of the chain segments in between consecutive crosslinks. Sidebottom [32,35] has shown that this model can explain the compositional variation in m vs. $<n>$ for simple alkali phosphates and aluminophosphates along the metaphosphate ($NaPO_3$)-P_2O_5 join, where $<n>$ represents the number of bridging oxygen atoms per P atom in the structure. Specifically, as $<n>$ increases from 2 in alkali metaphosphates and approaches 2.4, m rapidly decreases from ~80 to ~30, beyond which further increase in $<n>$ up to 3 for pure P_2O_5 results only in a small decrease in m (Fig. 11). Here the PO_4 tetrahedra are "coarse-grained" and treated as rigid super-structural units, which then do not contribute individually to the conformational entropy and only contributions from the inter-tetrahedral conformational changes need to be considered. This hypothesis in the CGM is based on the assumption that these rigid

structural units do not undergo significant deformation in response to an applied shear, instead majority of the deformation is taken up by the linkages between these units.

Recent rheological studies have shown that compared to alkali metaphosphates, Zn-metaphosphate is characterized by stronger cross-linking of the metaphosphate chains via Zn-O tetrahedra, which would likely impose strong restrictions on the chain reorientation and lower its conformational entropy [37]. Therefore, the conformational entropy only becomes a function of $\langle n \rangle$ once the Q^2 chains start shortening with further increase in the ZnO content beyond the metaphosphate composition and the steric hindrance towards chain conformation is lifted. Moreover, as shown in the present study, the Zn CN monotonically increases with increasing Zn content in this composition range and Zn increasingly assumes the role of a conventional network modifier. These effects, when taken together, are indeed consistent with the observation that m of Zn-phosphate glasses starts to increase with Zn content only in the polyphosphate composition region with >50 mol% ZnO (Fig. 11).

4. Summary

The compositional evolution of the structure of binary Zn-phosphate glasses is investigated using ^{31}P MAS and ^{67}Zn QMAT NMR spectroscopy. The phosphorus Q-speciation is found to be nearly binary. With increasing ZnO, the phosphate network becomes depolymerized with the gradual replacement of Q^3 and Q^2 species by a more closely packed structure constituted of Q^2 and Q^1 species, which leads to a lowering of the molar volume and T_g in the composition range 35 mol% $\leq$ ZnO $\leq$ 55 mol%. Further increase in the ZnO content results in a shortening of the Q^2 chains and lifting of their conformational constraints, as evidenced in the progressive lowering of the magnitude of ^{31}P CSA parameter Δ for the Q^2 species. Such structural changes of the Zn-phosphate network in these polyphosphate

compositions result in a rapid increase of the atomic packing density and fragility index due to a lowering of the steric hindrance of Q^2 chains. On the other hand, the ^{67}Zn QMAT NMR spectra indicate the presence of tetrahedral and octahedral Zn coordination environments in all glasses. The relative fraction of the octahedral environment and hence, the average Zn CN is observed to increase with increasing ZnO content beyond 40 mol%. The resulting rise in the average structural connectivity appears to compensate for the depolymerization of the phosphate network in the polyphosphates, which is manifested in a reversal of the compositional trend in T_g.

ACKNOWLEDGEMENT

This work is supported by the National Science Foundation Grant NSF DMR 1855176. The National High Magnetic Field Laboratory (NHMFL) in Tallahassee, FL, USA, is supported by NSF DMR-1644779 and the State of Florida.

References

[1] R.K. Brow, Review: the structure of simple phosphate glasses, J. Non. Cryst. Solids. 263&264 (2000) 1–28.

[2] R.K. Brow, T.M. Alam, D.R. Tallant, R.J. Kirkpatrick, Spectroscopic studies on the structures of phosphate sealing glasses, MRS Bull. 23 (1998) 63–67.

[3] M. Reza Dousti, R.J. Amjad, Spectroscopic properties of Tb^{3+}-doped lead zinc phosphate glass for green solid state laser, J. Non. Cryst. Solids. 420 (2015) 21–25.

[4] J. Juárez-Batalla, A.N. Meza-Rocha, G.H. Muñoz, I. Camarillo, U. Caldiño, Luminescence properties of Tb^{3+}-doped zinc phosphate glasses for green laser application, Opt. Mater. (Amst). 58 (2016) 406–411.

[5] L.B. Fletcher, J.J. Witcher, N. Troy, S.T. Reis, R.K. Brow, R.M. Vazquez, R. Osellame, D.M. Krol, Femtosecond laser writing of waveguides in zinc phosphate glasses, Opt. Mater. Express. 1 (2011) 845–855.

[6] B. Zhang, Q. Chen, L. Song, H. Li, F. Hou, The influence of Sb2O3 addition on the properties of low-melting ZnO-P2O5 glasses, J. Am. Ceram. Soc. 91 (2008) 2036–2038.

[7] G. Walter, U. Hoppe, J. Vogel, G. Carl, P. Hartmann, The structure of zinc polyphosphate glass studied by diffraction methods and ^{31}P NMR, J. Non. Cryst. Solids. 333 (2004) 252–262.

[8] J.W. Wiench, M. Pruski, B. Tischendorf, J.U. Otaigbe, B.C. Sales, Structural studies of zinc polyphosphate glasses by nuclear magnetic resonance, J. Non. Cryst. Solids. 263&264 (2000) 101–110.

[9] U. Hoppe, A. Saitoh, G. Tricot, P. Freudenberger, A.C. Hannon, H. Takebe, R.K. Brow, The structure and properties of $xZnO–(67-x)SnO–33P_2O_5$ glasses: (II) Diffraction, NMR, and chromatographic studies, J. Non. Cryst. Solids. 492 (2018) 68–76.

[10] K. Meyer, Characterization of the structure of binary zinc ultraphosphate glasses by infrared and Raman spectroscopy, 1997.

[11] B.C. Tischendorf, T.M. Alam, R.T. Cygan, J.U. Otaigbe, The structure and properties of binary zinc phosphate glasses studied by molecular dynamics simulations, J. Non. Cryst. Solids. 316 (2003) 261–272.

[12] B. Tischendorf, J.U. Otaigbe, J.W. Wiench, M. Pruski, B.C. Sales, A study of short and intermediate range order in zinc phosphate glasses, J. Non. Cryst. Solids. 282 (2001) 147–158.

[13] R.K. Brow, D.R. Tallant, S.T. Myers, C.C. Phifer, The short-range structure of zinc polyphosphate glass, J. Non. Cryst. Solids. 191 (1995) 45–55.

[14] K. Suzuya, K. Itoh, A. Kajinami, C.-K. Loong, The structure of binary zinc phosphate glasses, J. Non. Cryst. Solids. 345&346 (2004) 80–87.

[15] E. Kordes, W. Vogel, R. Feterowsky, Physical chemistry investigations of the

characteristics and fine structures of phosphate glasses, Z. Elektrochem. 57 (1953) 282–289.

[16] U. Hoppe, G. Walter, R. Kranold, D. Stachel, A. Barz, The dependence of structural peculiarities in binary phosphate glasses on their network modifier content, J. Non. Cryst. Solids. 192–193 (1995) 28–31.

[17] R.S.K. Madsen, A. Qiao, J. Sen, I. Hung, K. Chen, Z. Gan, S. Sen, Y. Yue, Ultrahigh-field ^{67}Zn NMR reveals short-range disorder in zeolitic imidazolate framework glasses, Science (80-.). 367 (2020) 1473–1476.

[18] Y. Zhang, S. Mukheriee, E. Oldfield, ^{67}Zn NMR chemical shifts and electric field gradients in zinc complexes: A quantum chemical investigation, J. Am. Chem. Soc. 127 (2005) 2370–2371.

[19] G. Wu, Zinc-67 nuclear magnetic resonance spectroscopy of solids, Chem. Phys. Lett. 298 (1998) 375–380.

[20] I. Hung, Z. Gan, A magic-angle turning NMR experiment for separating spinning sidebands of half-integer quadrupolar nuclei, Chem. Phys. Lett. 496 (2010) 162–166.

[21] Y. Xia, B. Yuan, O. Gulbiten, B. Aitken, S. Sen, Kinetic and calorimetric fragility of chalcogenide glass-forming liquids: Role of shear vs enthalpy relaxation, J. Phys. Chem. B. 125 (2021) 2754–2760.

[22] D. Massiot, F. Fayon, M. Capron, I. King, S. Le Calvé, B. Alonso, J.O. Durand, B. Bujoli, Z. Gan, G. Hoatson, Modelling one- and two-dimensional solid-state NMR spectra, Magn. Reson. Chem. 40 (2002) 70–76.

[23] Z. Gan, I. Hung, X. Wang, J. Paulino, G. Wu, I.M. Litvak, P.L. Gor'kov, W.W. Brey, P. Lendi, J.L. Schiano, M.D. Bird, I.R. Dixon, J. Toth, G.S. Boebinger, T.A. Cross, NMR spectroscopy up to 35.2 T using a series-connected hybrid magnet, J. Magn. Reson. 284 (2017) 125–136.

[24] F.H. Larsen, H.J. Jakobsen, P.D. Ellis, N.C. Nielsen, Sensitivity-Enhanced Quadrupolar-Echo NMR of Half-Integer Quadrupolar Nuclei. Magnitudes and Relative Orientation of Chemical Shielding and Quadrupolar Coupling Tensors, 101 (1997) 8597–8606.

[25] D.J. States, R.A. Haberkorn, D.J. Ruben, A Two-Dimensional Nuclear Overhauser Experiment with Pure Absorption Phase in Four Quadrants, J. Magn. Reson. 48 (1982) 286–292.

[26] I. Hung, T. Edwards, S. Sen, Z. Gan, MATPASS/CPMG: A sensitivity enhanced magic-angle spinning sideband separation experiment for disordered solids, J. Magn. Reson. 221 (2012) 103–109.

[27] R.K. Harris, E.D. Becker, S.M.C. de Menezes, R. Goodfellow, Pierre Granger, NMR Nomenclature. Nuclear Spin Properties And Conventions For Chemicals Shifts, 73 (2001) 1795–1818.

[28] P. Zhang, P.J. Grandinetti, J.F. Stebbins, Anionic Species Determination in $CaSiO_3$ Glass Using Two-Dimensional ^{29}Si NMR, J. Phys. Chem. B. 101 (1997) 4004–4008.

[29] S.G.J. van Meerten, W.M.J. Franssen, A.P.M. Kentgens, ssNake: A cross-platform open-source NMR data processing and fitting application, J. Magn. Reson. 301 (2019) 56–66.

[30] M. Bionducci, G. Lichen, A. Musinu, G. Navarra, G. Piccaluga, G. Pinna, The structure of a Zn(II) metaphosphate glass. I. The cation coordination by a Combination of X-Ray and Neutron diffraction, EXAFS and X-Ray anomalous scattering, Z. Naturforsch. 51 (1996) 1209–1215.

[31] R. Fabian, D.L. Sidebottom, Dynamic light scattering in network-forming sodium ultraphosphate liquids near the glass transition, Phys. Rev. B - Condens. Matter Mater. Phys. 80 (2009) 064201.

[32] D.L. Sidebottom, Fragility of network-forming glasses: A universal dependence on the topological connectivity, Phys. Rev. E. 92 (2015) 062804.

[33] D.L. Sidebottom, S.E. Schnell, Role of intermediate-range order in predicting the fragility of network-forming liquids near the rigidity transition, Phys. Rev. B. 87 (2013) 054202.

[34] D.L. Sidebottom, T.D. Tran, S.E. Schnell, Building up a weaker network: The effect of intermediate range glass structure on liquid fragility, J. Non. Cryst. Solids. 402 (2014) 16–20.

[35] D.L. Sidebottom, Connecting glass-forming fragility to network topology, Front. Mater. 6 (2019) 144.

[36] D.L. Sidebottom, The fragility of alkali silicate glass melts: Part of a universal topological pattern, J. Non. Cryst. Solids. 516 (2019) 63–66.

[37] Y. Xia, H. Chen, B. Aitken, S. Sen, Rheological characterization of complex dynamics in Na-Zn metaphosphate glass-forming liquids, J. Chem. Phys. 155 (2021) 054503.

[38] B.C. Sales, J.U. Otaigbe, G.H. Beall, L.A. Boatner, J.O. Ramey, Structure of zinc polyphosphate glasses, J. Non. Cryst. Solids. 226 (1998) 287–293.

[39] M. Ouchetto, B. Elouadi, S. Parke, Study of lanthanide zinc phosphate glasses by differential thermal analysis, Phys. Chem. Glas. 32 (1991) 22–28.

Table 1. Chemical shift and quadrupolar parameters used for two-site simulation of ^{67}Zn QMAT central transition NMR spectra of Zn-phosphate glasses collected at 35.2 T and at 19.6 T (top).

Glass composition and magnetic field	sites	δ_{iso} (±5 ppm)	average C_Q (±0.2 MHz)	average η	Czjzek width (MHz)	Relative fraction (±5 %)
$(ZnO)_{40}(P_2O_5)_{60}$	1	67	2.9	0	2.5	45%
19.6 T	2	0	3.8	0	3.8	55%
$(ZnO)_{40}(P_2O_5)_{60}$	1	65	3.0	0	3.0	50%
35.2 T	2	0	4.0	0	4.5	50%
$(ZnO)_{60}(P_2O_5)_{40}$	1	62	3.0	0	3.7	37%
35.2 T	2	–5	4.1	0	5.0	63%
$(ZnO)_{67}(P_2O_5)_{33}$	1	62	3.1	0	3.9	29%
35.2 T	2	–5	4.1	0	5.4	71%

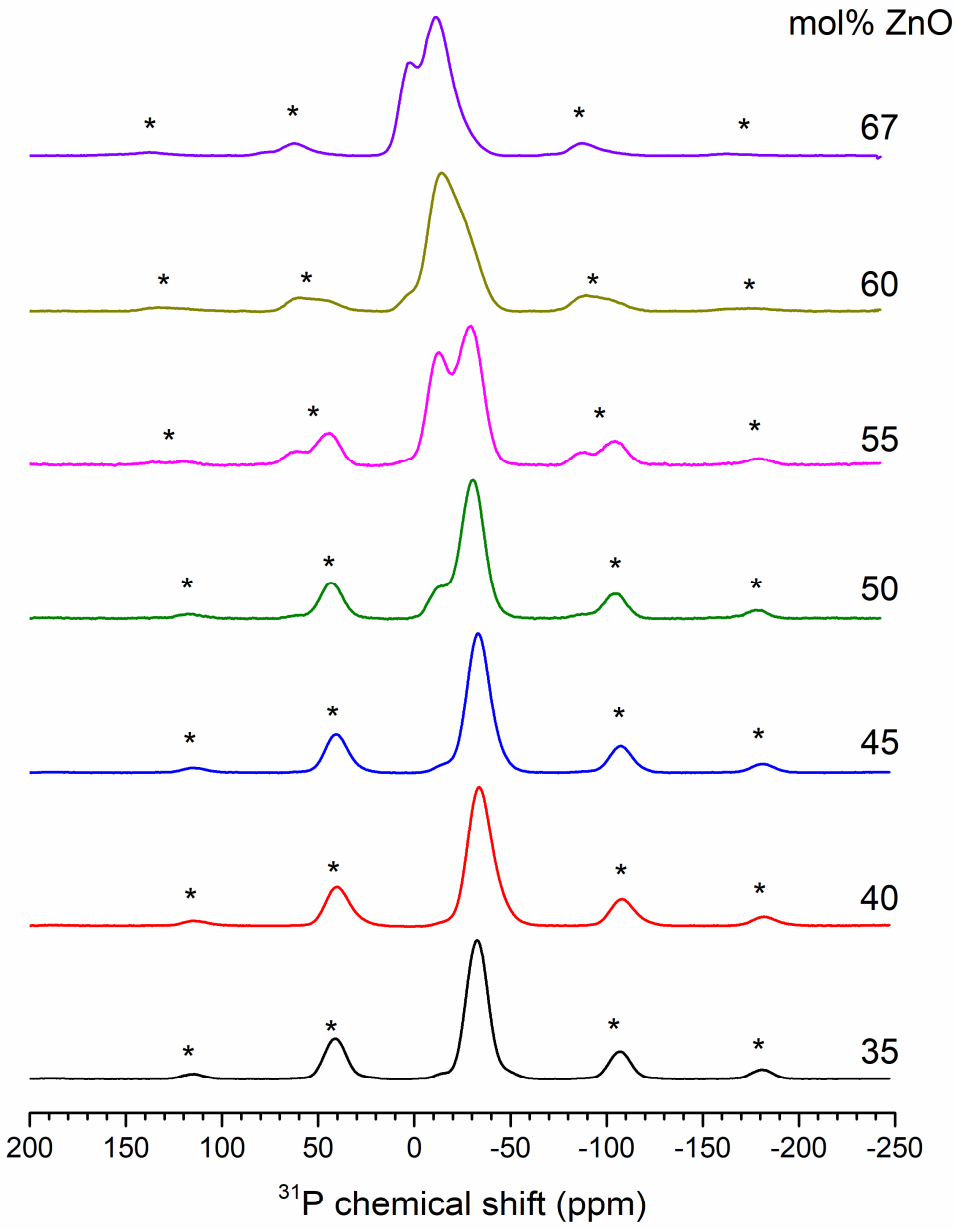

Figure 1. ^{31}P MAS NMR spectra of ZnO–P_2O_5 glasses. Glass composition in terms of mol% ZnO are shown alongside the spectra. Asterisks denote spinning sidebands.

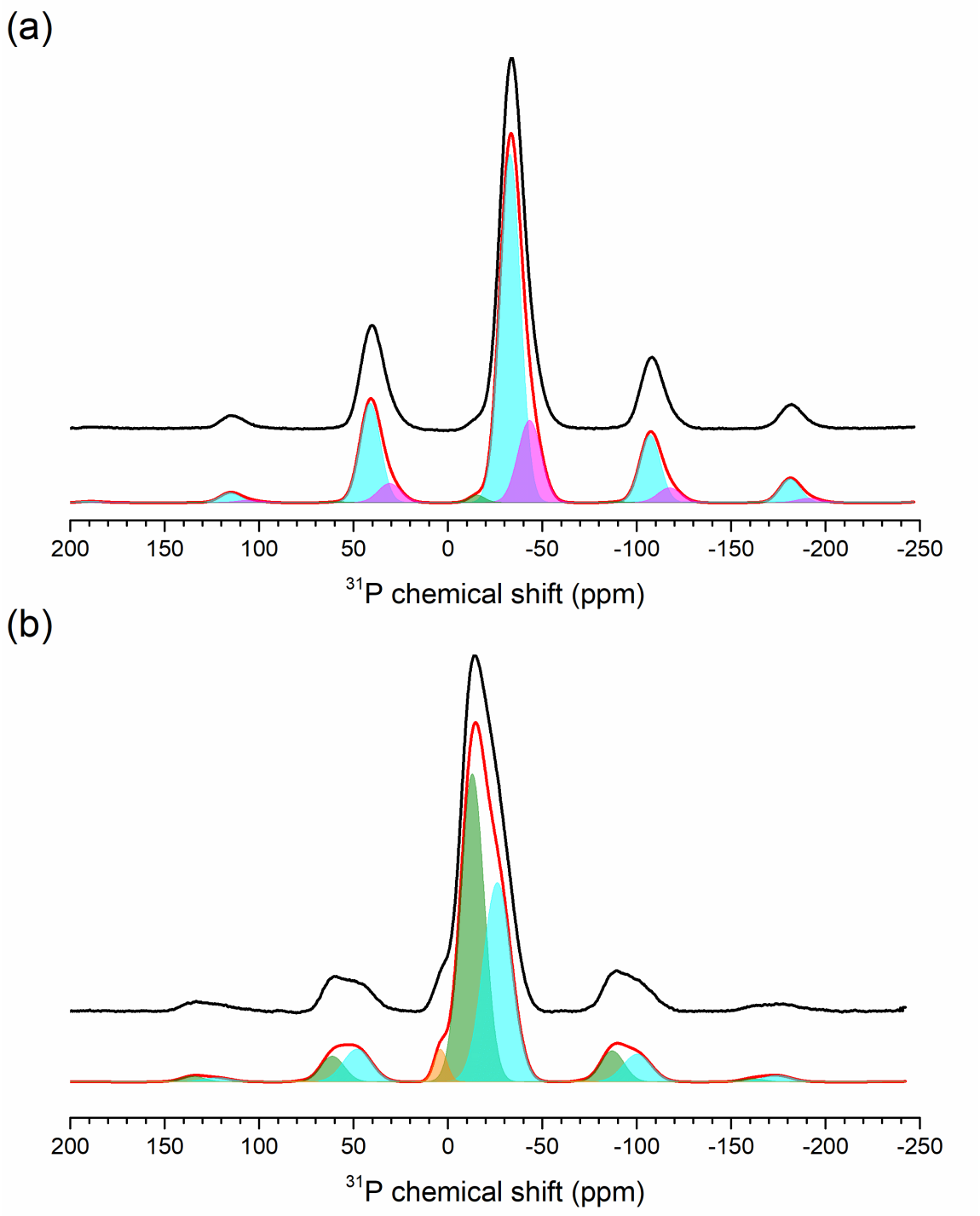

Figure 2. Representative simulations of ^{31}P MAS NMR spectral line shapes of (a) $40ZnO–60P_2O_5$ and (b) $60ZnO–40\ P_2O_5$ glasses. Experimental (black) and simulated (red) line shapes are shown along with the Gaussian simulation components corresponding to various Q species: Q^0 (orange); Q^1 (green); Q^2 (teal); and Q^3 (magenta).

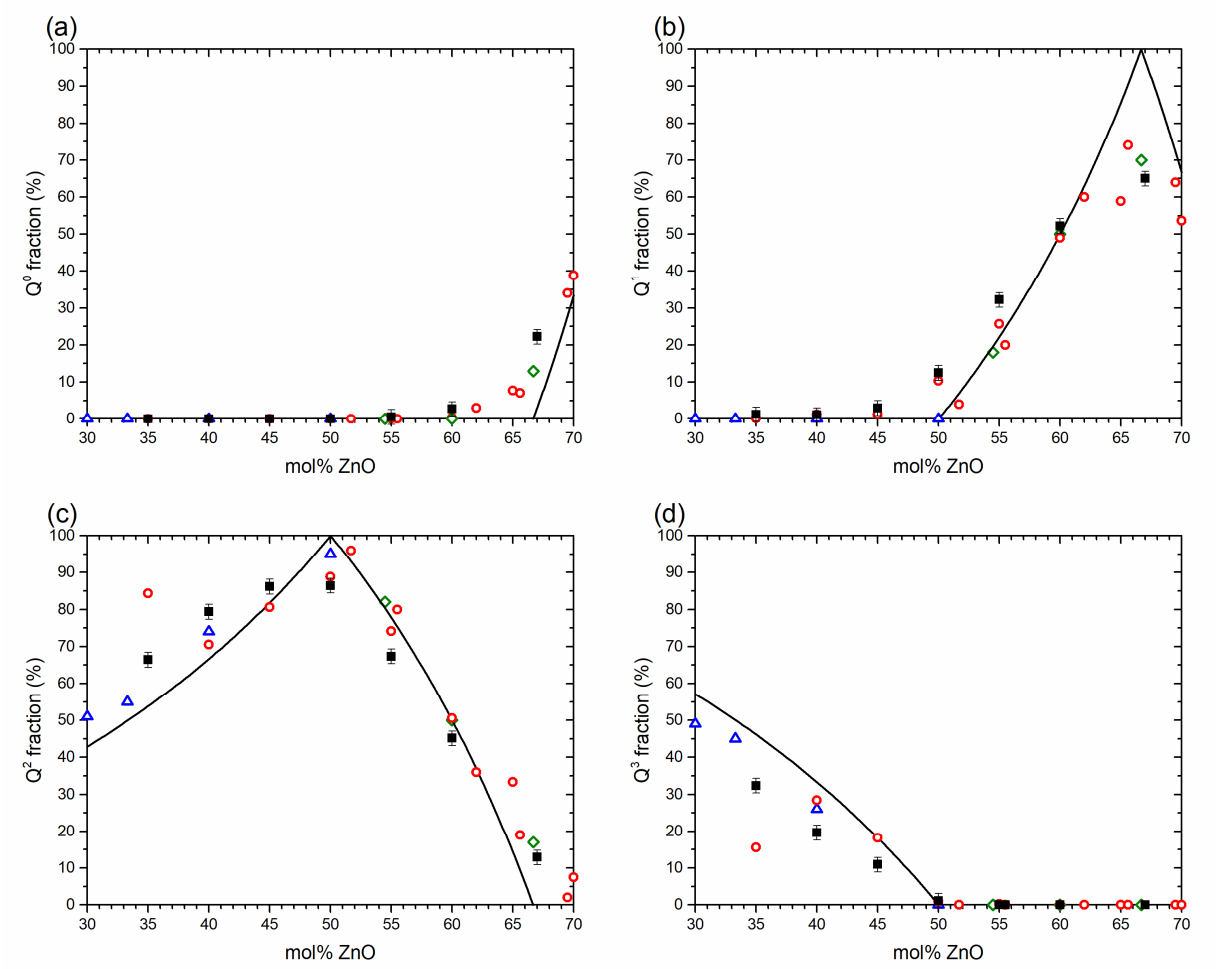

Figure 3. Composition dependence of relative fraction of (a) Q^0; (b) Q^1; (c) Q^2 and (d) Q^3 species in Zn-phosphate glasses determined in the present study from simulation of ^{31}P NMR spectra (filled squares). Literature results (open symbols) reported by Wiench et al. (red circles) [8], Sales et al. (green diamonds) [38] and Meyer (blue triangles) [10] are shown for comparison. Solid lines are predicted fractions according to van Wazer's binary model.

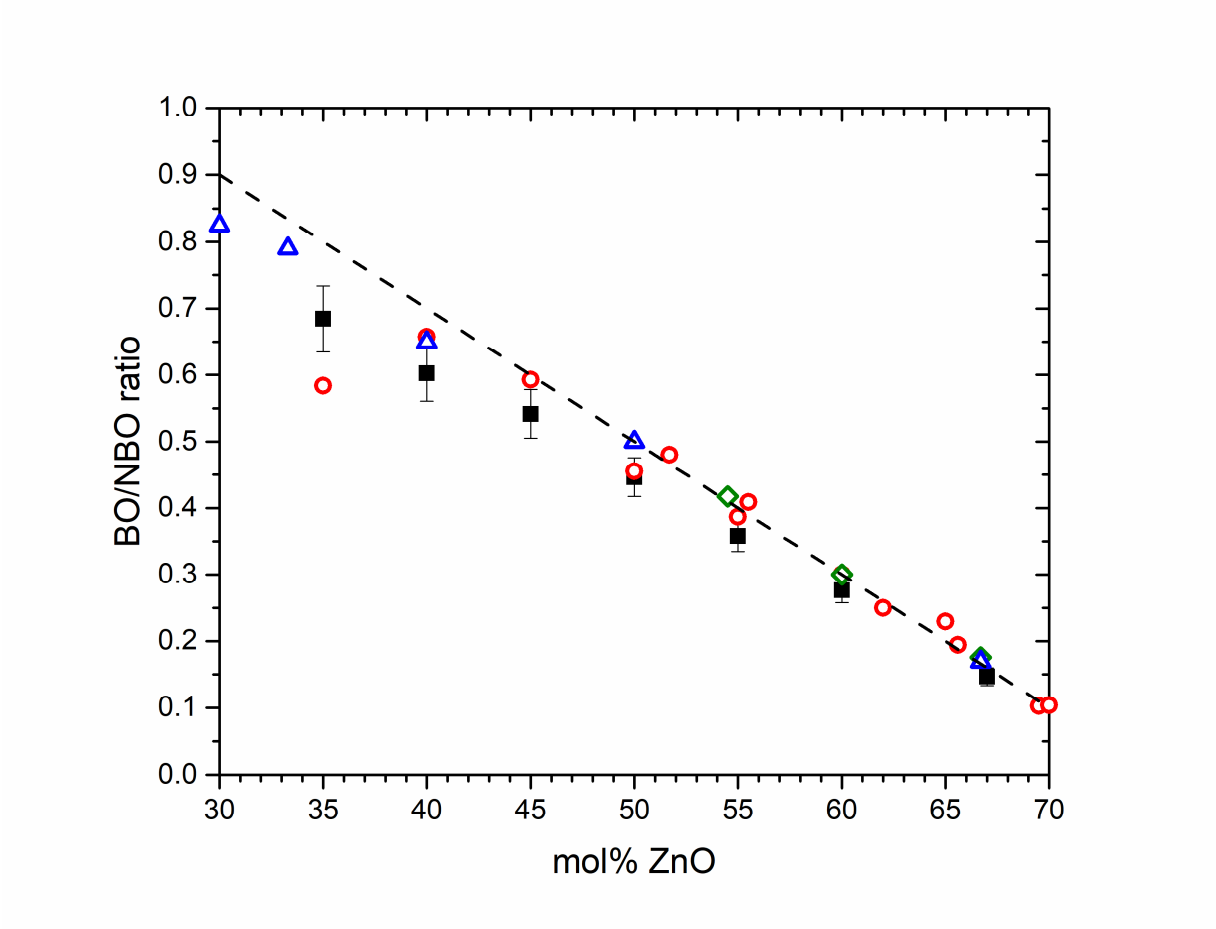

Figure 4. Comparison between BO/NBO ratio of $ZnO–P_2O_5$ glasses determined in the present study from Q^n speciation (filled squares) and those reported literature by Wiench et al. (red circles) [8], Sales et al. (green diamonds) [38] and Meyer (blue triangles) [10]. Dashed line corresponds to expected values from nominal composition.

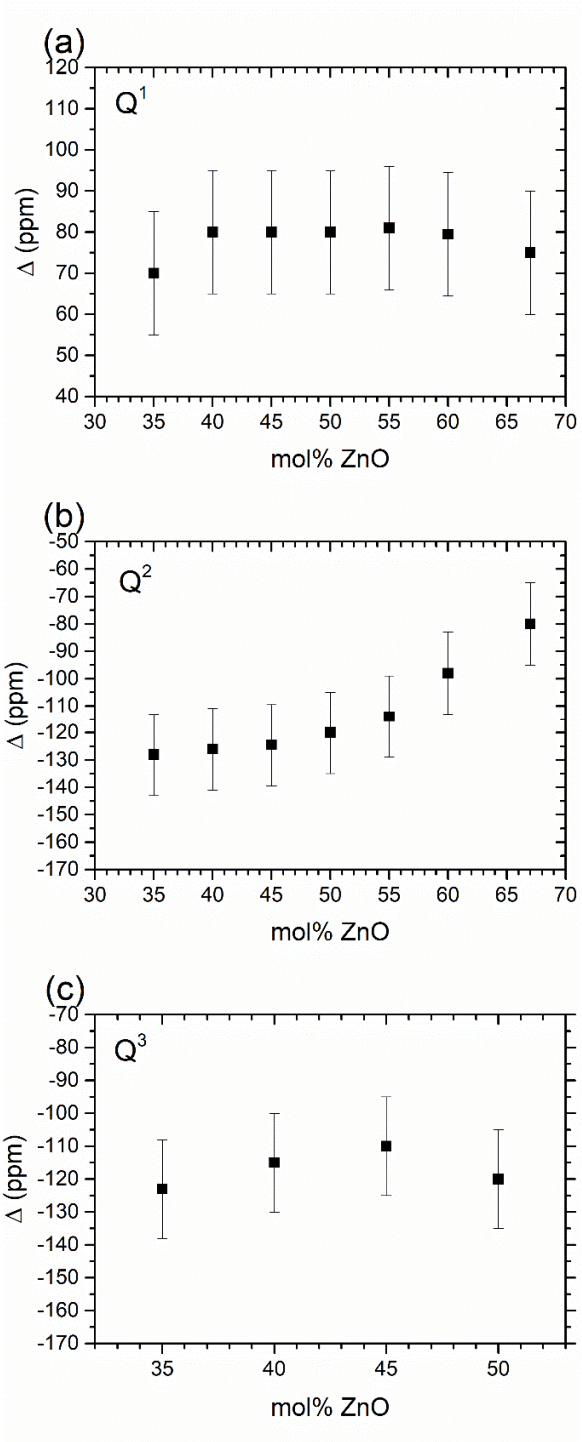

Figure 5. Compositional variation of Δ for (a) Q^1, (b) Q^2 and (c) Q^3 species in $ZnO–P_2O_5$ glasses.

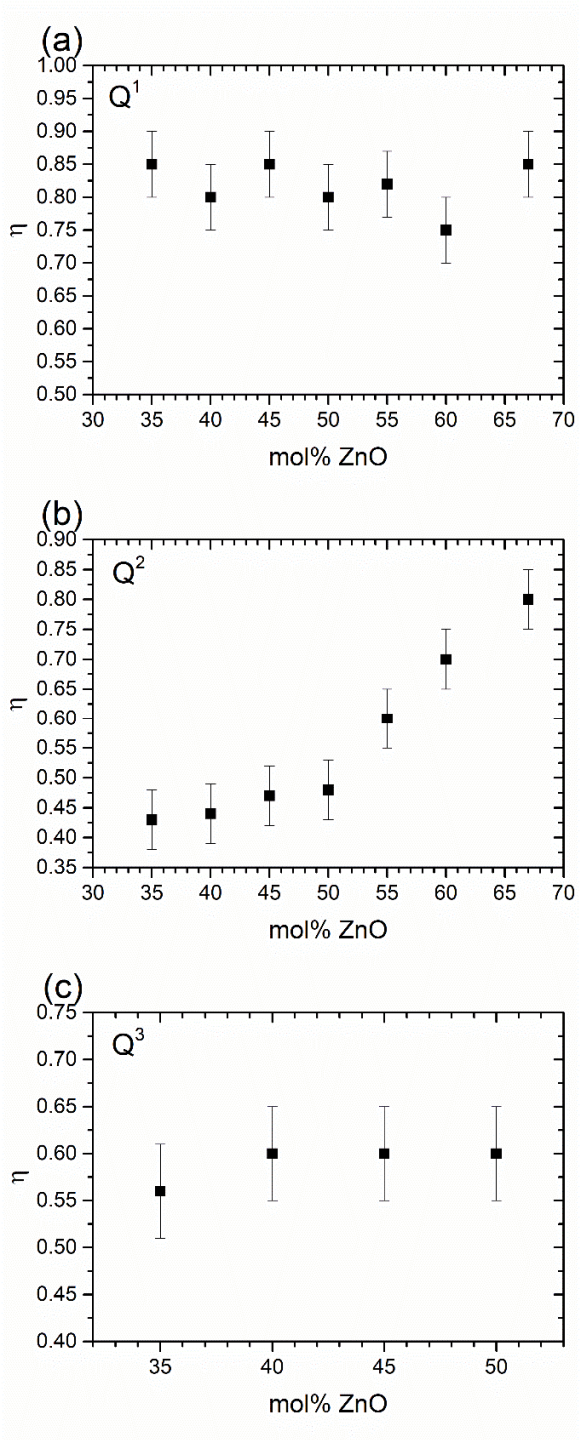

Figure 6. Compositional variation of η for (a) Q^1, (b) Q^2 and (c) Q^3 species in ZnO–P_2O_5 glasses.

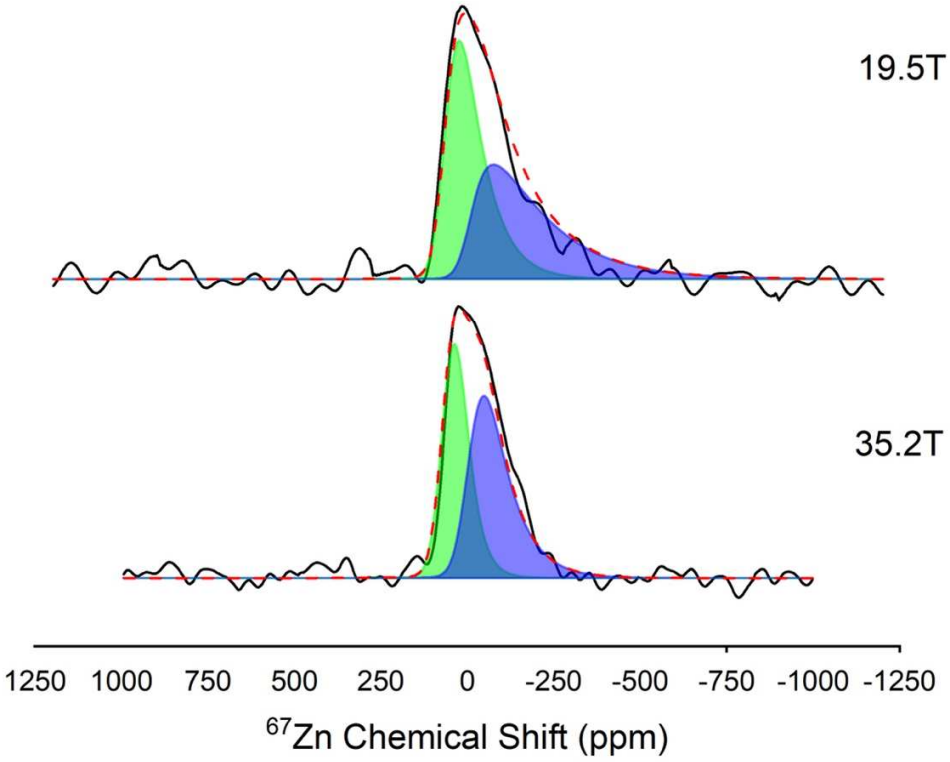

Figure 7. Two-site simulation of ^{67}Zn QMAT central transition NMR spectra of $(ZnO)_{40}(P_2O_5)_{60}$ glass collected at 35.2 T (bottom) and at 19.6 T (top). Experimental (solid black line) and simulated (red dashed line) line shapes are shown along with the two simulation components (blue and green peaks). Simulation parameters are listed in Table 1.

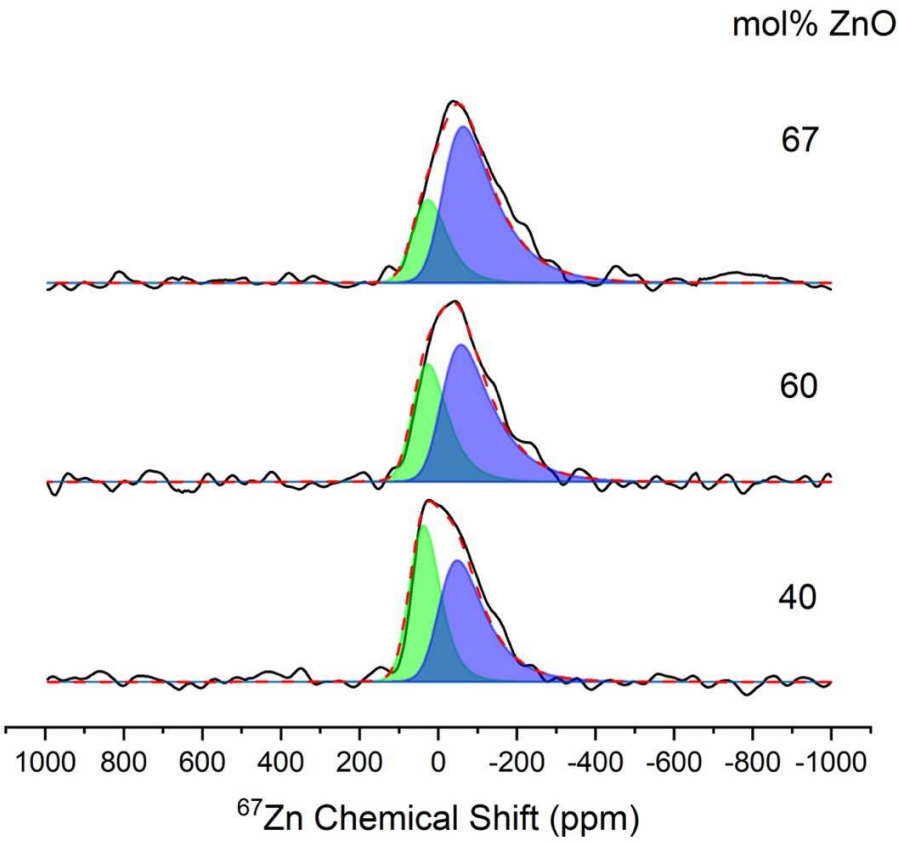

Figure 8. Two-site simulation of ^{67}Zn QMAT central transition NMR spectra of ZnO–P_2O_5 glasses collected at 35.2 T. Glass compositions in terms of mol% ZnO are shown alongside the spectra. Experimental (solid black line) and simulated (red dashed line) line shapes are shown along with the two simulation components (blue and green peaks). Simulation parameters are listed in Table 1.

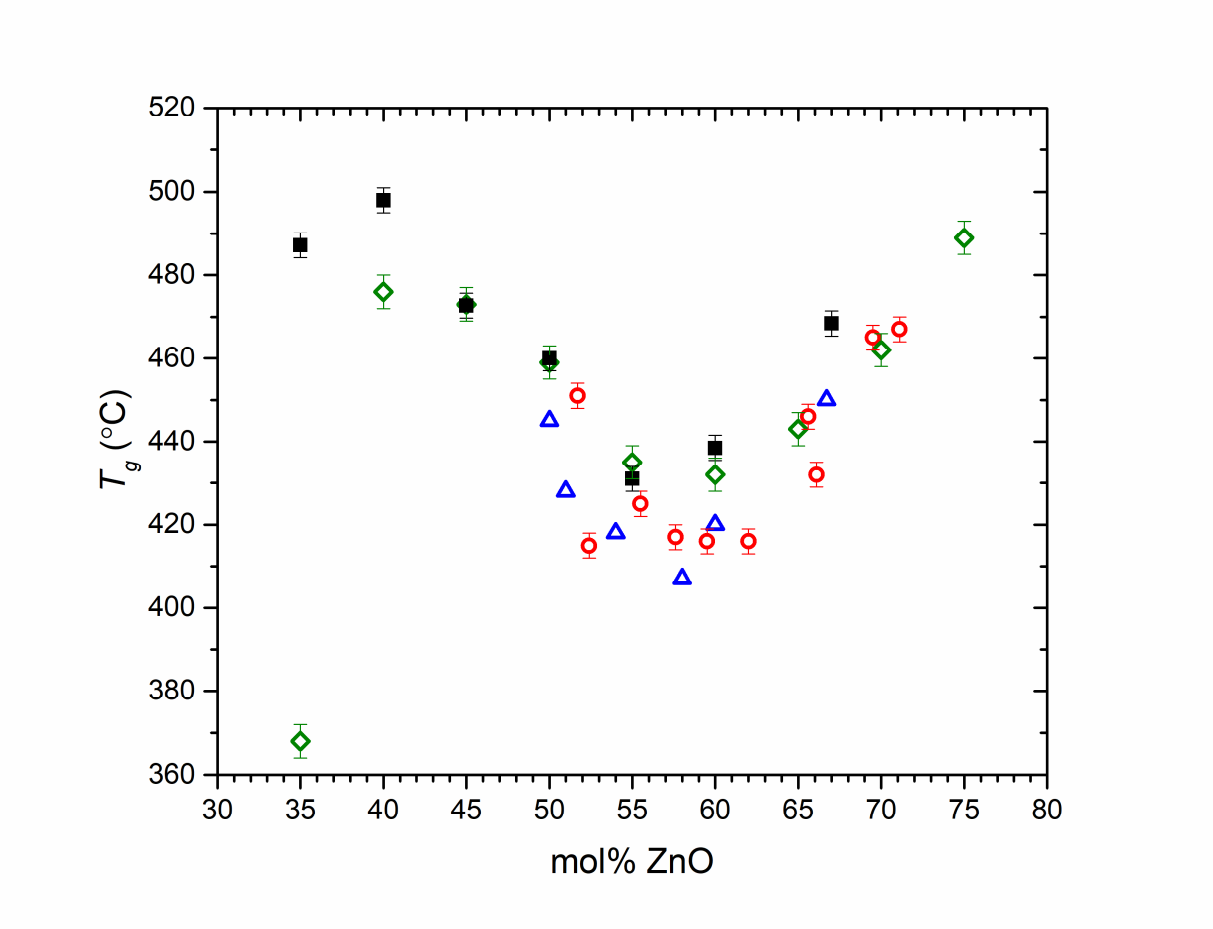

Figure 9. Glass transition temperature of $ZnO–P_2O_5$ glasses measured in the present study (filled squares). Literature results reported by Brow et al. (red circles) [13], Tischendorf et al. (green diamonds) [12] and Ouchetto et al. (blue triangles) [39] are shown for comparison.

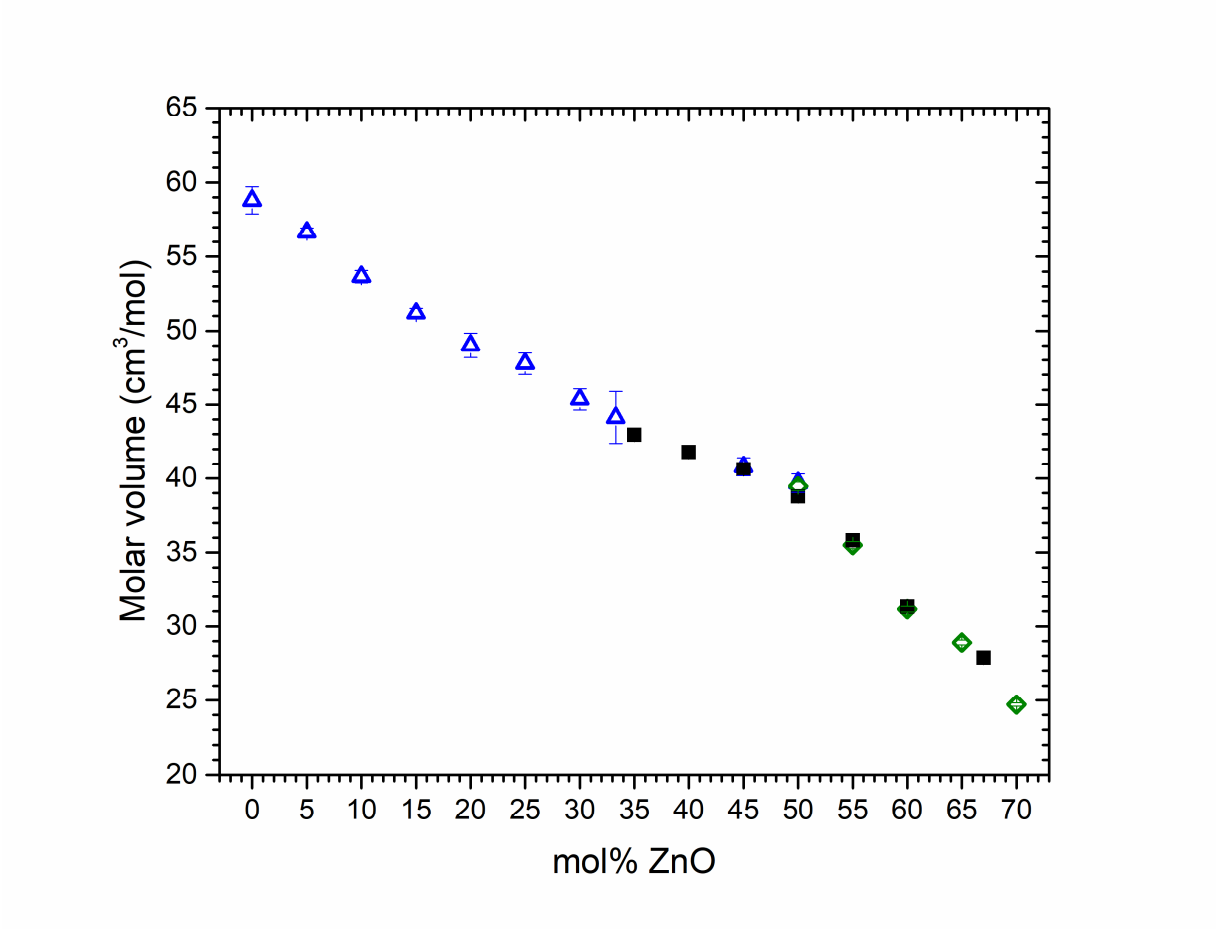

Figure 10. Molar volume of $ZnO–P_2O_5$ glasses measured in the present study (filled squares). Literature results reported by Tischendorf et al. (green diamonds) [11] and Meyer (blue triangles) [10] are shown for comparison.

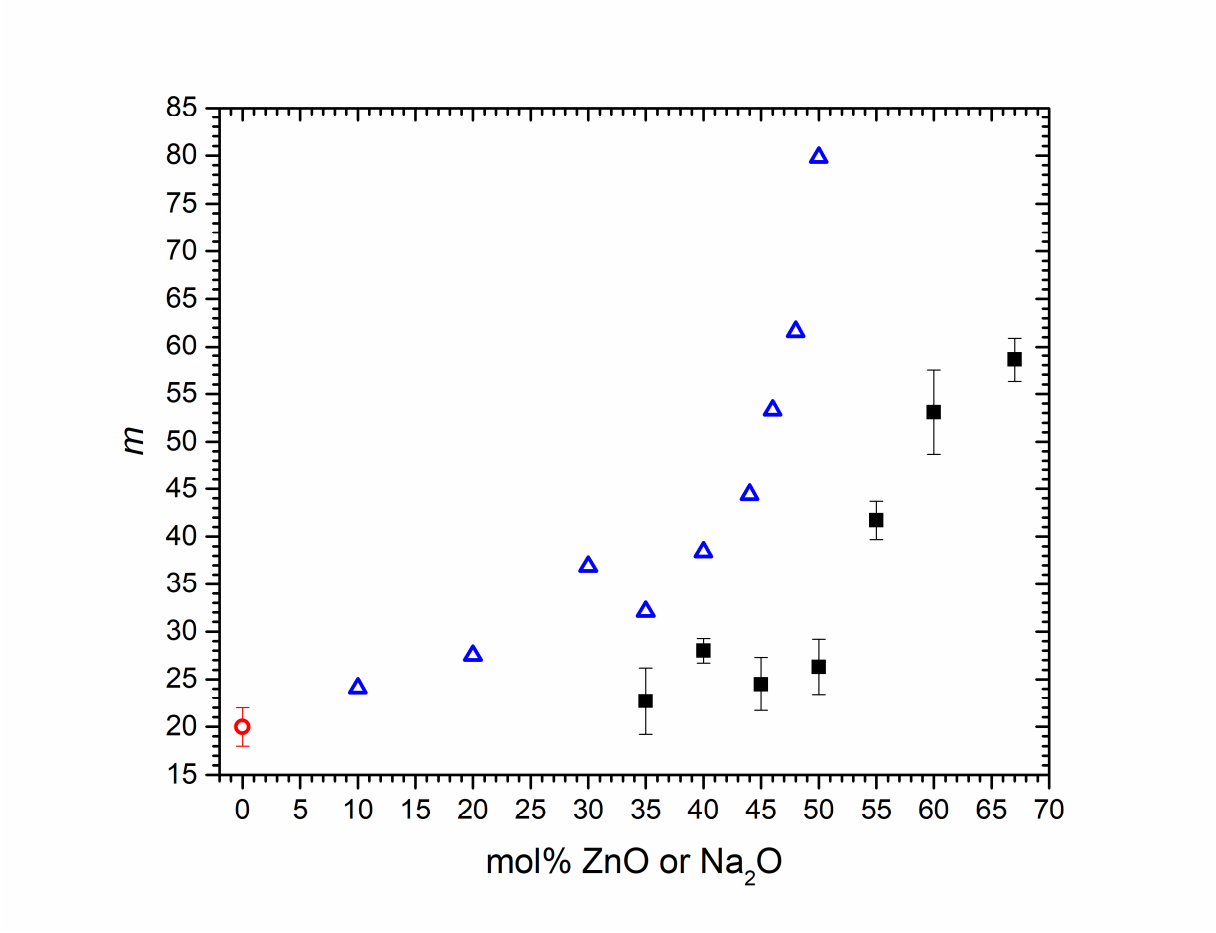

Figure 11. Fragility indices of $ZnO–P_2O_5$ glasses (filled squares) determined in the present study, and of P_2O_5 (red circle) and $Na_2O–P_2O_5$ (blue triangles) glasses reported in the literature [31].